SANDIA REPORT
SAND2015-7320
Unlimited Release
Printed August 2015

C2R2: Compact Compound Recirculator/Recuperator for Renewable Energy and Energy Efficient Thermochemical Processing

Ivan Ermanoski, Adrian Orozco

Prepared by
Sandia National Laboratories
Albuquerque, New Mexico 87185 and Livermore, California 94550

Sandia National Laboratories is a multi-program laboratory managed and operated by Sandia Corporation, a wholly owned subsidiary of Lockheed Martin Corporation, for the U.S. Department of Energy's National Nuclear Security Administration under contract DE-AC04-94AL85000.

Issued by Sandia National Laboratories, operated for the United States Department of Energy by Sandia Corporation.

Available to DOE and DOE contractors from
U.S. Department of Energy
Office of Scientific and Technical Information
P.O. Box 62
Oak Ridge, TN 37831

Telephone: (865) 576-8401
FaCNCmile: (865) 576-5728
E-Mail: reports@osti.gov
Online ordering: http://www.osti.gov/scitech

Available to the public from
U.S. Department of Commerce
National Technical Information Service
5301 Shawnee Rd
Alexandria, VA 22312

Telephone: (800) 553-6847
FaCNCmile: (703) 605-6900
E-Mail: orders@ntis.gov
Online order: http://www.ntis.gov/search

SAND2015-7320
Unlimited Release
Printed August 2015

C2R2: Compact Compound Recirculator/Recuperator for Renewable Energy and Energy Efficient Thermochemical Processing

Ivan Ermanoski and Adrian Orozco
Materials, Devices & Energy Technologies Department
Sandia National Laboratories
P.O. Box 5800
Albuquerque, New Mexico 87185-MS145

Abstract

In this report we present the development of a packed particle bed recirculator and heat exchanger. The device is intended to create countercurrent flows of packed particle beds and exchange heat between the flows. The project focused on the design, fabrication, demonstration, and modifications of a simple prototype, in order to attain high levels of heat exchange between particle flows while maintaining an effective particle conveying rate in a scalable package. Despite heat losses in a package not optimized for heat retention, 50% heat recovery was achieved, at a particle conveying efficiency of 40%.

ACKNOWLEDGMENTS

CONTENTS

FIGURES

TABLES

NOMENCLATURE

C2R2	Compact Compound Recirculator/Recuperator
CNC	Conventional Cutter
DAQ	Data Acquisition Device
I.D.	Inner Diameter
O.D.	Outer Diameter
PE	Particle Elevator
SS	Stainless Steel
TC	Thermocouple
ZPC	Zero-Profile Cutter

1. INTRODUCTION

1.1. Motivation

While fluid-fluid and fluid-bulk solid heat exchangers are ubiquitous in today's world (from microelectronics to massive power plants), the challenging, yet promising field of heat exchange between packed particle beds, remains almost entirely unexplored and undeveloped. Existing applications in need of this kind of heat exchange, such as cement manufacture, employ workarounds involving fluids to achieve satisfactory results. The need, however, has been steadily increasing in emerging technologies, such as solar coal and natural gas upgrade, solar-thermochemical energy storage, water and CO_2 capture, or solar-thermochemical fuel production, where workarounds would be difficult, if at all possible. These technologies will benefit significantly or depend critically on the development of heat exchangers for packed particle beds. This critical need is especially well documented in the field of solar fuels.[1, 2] Two key issues must be resolved before heat exchangers for packed particle beds can be deployed in real-world applications in general: (1) effectiveness and (2) scaling. The main goal of this project was the experimental demonstration of particle conveying and heat exchange in a scalable package: the *compact compound recirculator/recuperator* (C2R2).

1.2. Outstanding issues, and potential solutions

The difficulty in exchanging heat between packed particle beds stems from a combination of properties that make them similar to both solids and liquids in an unusually unfavorable way. The first factor is their exceptionally low thermal conductivity, which is roughly two orders of magnitude lower than the constituent bulk solid, and is primarily the result of contact conductivity between particles.[3] Thermal conductivity is especially low in static beds, which are excellent thermal insulators, with thermal conductivities orders of magnitude lower than the corresponding bulk solid. The numerous interparticle contacts over any appreciable length effectively add resistance to heat transfer, leading to poor thermal conductivity. In addition, convective heat transfer of gases in the voids within the bed partly contributes to the overall conductivity, making heat transfer at low gas pressures (a necessity for some applications) even more challenging. The reverse, however, is not true, i.e. bed thermal conductivity cannot be increased appreciably by increasing the system pressure, even if such an increase is otherwise inherently beneficial for the application in question.[3] Finally, heat transfer via blackbody radiation between particles contributes negligibly to the overall conductivity at low temperature, but has not been well characterized at high temperature.[3]

The thermal conductivity of static packed beds is also universally low, almost irrespective of the constituent material of the particles themselves. [4-6] Thermal conductivity measurements of static packed beds are difficult, and require thorough experimental control and an accounting for thermal bridging and other interfering phenomena. Typical values are in the range of 0.1-0.5W/mK, vastly smaller than good thermal conductors, typically used in heat exchangers, such as copper (k=401W/mK) or aluminum (k=205W/mK), or typical construction materials such as steel (k=43W/mK). The thermal conductivity of static particle beds is small even when compared with materials that are typically thought of as thermal insulators (e.g. for aluminum

oxide k=30W/mK). With such low thermal conductivities in mind, even a simple estimate of the potential for heat exchange in static particle beds will show that it is feasible, however inefficiently, only for very short transport distances of less than 5mm.
These properties of packed particle beds resemble those of bulk solids (almost purely conductive heat transfer) with a very low coefficient of thermal conductivity, comparable to the best insulating materials.

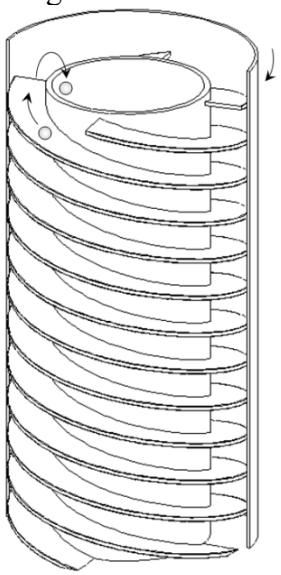

Figure 1. SD# 12568 illustration. Particles are moved up the stationary auger, as a packed bed, by the rotation of the casing.

Particle beds also resemble liquids, in the sense that they can "flow", the hourglass being the most easily visualized example. However, they do not share other properties of liquids, most importantly, internal convection and isotropic pressure under static conditions. The lack of internal convection (common in fluids) contributes to the low coefficient of thermal conductivity of packed particle beds. Furthermore, moving particle beds can form arches, both interlocking (large particles locking together) and cohesive (fine particles adhering to each other), which arrest flow. For these reasons, it is impossible to pump packed particle beds through narrow pipes (and for the most part through pipes at all) or through other heat exchange structures (e.g. fins)—a technique frequently used in fluid-fluid heat exchangers to achieve the maximum exchange in a small package. Particle beds can be pumped only by fluidization, which requires the introduction of a motive fluid into the system, and is incompatible with many of the applications enumerated in the introduction. The most commonly used methods for packed particle transport (e.g. bucket elevators, screw conveyors, belt conveyors, etc.) are also almost entirely incompatible with heat recovery. Bulk powders are not solid either, i.e. they cannot be moved through a system by attachment to a conveying system.

To solve the problem of bed-bed heat exchange, we relied on two elements. The first is a technical advance in conveying packed particle beds in a fashion compatible with high heat recovery effectiveness (SD# 12568), schematically illustrated in Figure 1. This invention is based on a particle elevator (Olds elevator), with a stationary auger and a rotating outside casing. This elevator type lends itself very well to the application demands because, among other benefits, it is mechanically simple, conveys material in the form of a full bore densely packed bed, has a high vertical conveying efficiency, and allows precise volumetric flow control.
The drawback of low thermal conductivity of particle beds is offset by the innovative multi helix auger geometry that minimizes thermal diffusion lengths, and increases the effective thermal conductivity of the bed (compared to static conditions) by creating an internal convective motion. The downward flow of particles is constrained to the region near the inside diameter of the auger shaft, enabling heat exchange between the two countercurrent flows. In existing elevators, the augers typically have only one helix (flight) that extend close to the center of the shaft, and have a roughly 1:1 pitch/diameter ratio: optimal for particle transport, but of virtually no use for heat exchange.

Preliminary experiments in a minimum configuration "benchtop" prototype (double helix auger), showed that the auger design is sound and, despite the unusual geometry, capable of conveying particles. Calculations based on a simple heat transfer model show the potential for high degrees of heat exchange, in excess of 80% at the 100kW power level in large units. These results also point to the main limitation of the approach—its scaling property. The capacity of the conveyor/recuperator is proportional to its diameter and length (i.e. its surface area), as opposed to its volume. This is caused by the effective use of only the device periphery or "skin" (Figure 1), but not the entire internal volume. One of the challenges is to overcome the scaling limitation (i.e. design a compact device, by using the entire volume to the greatest feasible extent), while accomplishing a high degree of heat recovery and maintaining mechanical simplicity.

Despite the unusual auger design, high levels of heat recovery appeared to be possible at the aforementioned short transfer distances of a few millimeters—assuming that the thermal conductivity of a packed but moving bed is similar to that of a static bed. Unfortunately, thermal conductivities of moving packed beds are very much an unknown, even though heat transfer rates have been measured. [4-6] Because of the multitude of dynamic and unknown bed properties in heat transfer experiments, no reliable values for thermal conductivity have been deduced. [4-6]

Considering the above limitations and considerations, to design a viable solid-solid heat recovery device, four main technical elements needed to be demonstrated:

- An auger design with minimal heat transfer lengths, which nonetheless is capable of efficient particle conveying;
- Particle conveying using zero or minimal profile inlets, such that they are compatible with the concentric nesting of multiple elements into a compact device;
- Design solutions for nesting multiple elevators, such that they can work simultaneously and efficiently, and;
- Heat transfer over distances longer than those indicated by the limitations of static beds.

The research and development with respect to all of these four elements is described in the following chapters.

1.3. General Experiment Information

To evaluate the four elements discussed above, the project was conducted in several stages. First, design multi-flight auger prototypes and evaluate of their conveying efficiencies (section 2). Second, the design and characterization of a cutter (Figure 2) compatible with a tightly nested auger system (section 4). Third, demonstrate the basic feasibility of a nested auger system (section 4). Finally, evaluate the heat exchange between counter-current flows of packed particle beds in the particle elevator (section 0). This section contains an overview of the experimental procedures and methods used in all experimental stages. A description of the particle elevator (Olds Elevator) is given in section 1.3.1. The general experimental setup is discussed in 1.3.2.

1.3.1. The Particle Elevator

The particle elevator (or Olds Elevator) is a vertical conveyor that consists of four major components: a stationary auger and hopper, and a rotating casing, at the bottom of which is a cutter. Figure 2 shows how these four components are arranged and how the material is conveyed through the elevator. The hopper holds the material while the cutters sweep it into the casing. A packed particle bed is conveyed up the stationary auger via frictional forces between the inner wall of the rotating casing and the conveyed material. In our experiments, a hollow shaft auger design allows the conveyed material to flow down through the shaft after reaching the top of the auger. This design produces a counter-current flow arrangement between the material conveyed up the auger and that flowing down the shaft. The rate at which the material is conveyed is known as the conveying rate and, for the Olds elevator, is directly proportional to the casing angular velocity [7], allowing precise control of volumetric flow. In practice, the conveying rate is also dependent on the bed depth (shown in Figure 2), which is the height of the sand above the cutters.

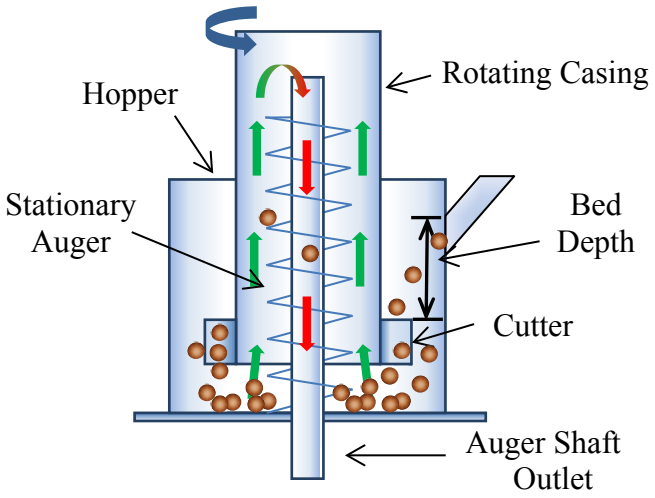

Figure 2. The diagram shows a cross section of the Olds Elevator. As the casing rotates, the cutters sweep the material into the casing driving a packed particle bed up the flights of a stationary auger (the image only shows a few of these particles for clarity). For this project, an auger with a hollow shaft was used to allow the material to flow down and out the auger shaft outlet after reaching the top of the auger.

1.3.2. Experimental Setup

The particle elevator (PE) experimental apparatus is shown in Figure 3. A permanent magnet DC motor (746W) and a worm gear system with a speed-reduction ratio of 1:40 were used to rotate the casing (Figure 4). The worm was slipped over the motor's drive shaft which was extended using a flexible shaft coupling. The casing was built with two parallel circular plates welded to a 8.9cm outer diameter (O.D.) cylinder, and was held in place by two stationary rectangular plates (Figure 4). Bearings were placed in grooves that were made in both the rectangular and circular plates. A motor speed controller was used to vary the casing angular velocity. A cylindrical hopper (2 in Figure 3a) was centered and bolted on top of a rectangular plate. A funnel bolted to the PE frame was connected to the hopper with a rubber hose (1 in Figure 3a) and was used to feed dry silica sand (<800 μm) into the hopper. The vertical position of the hose in the hopper is

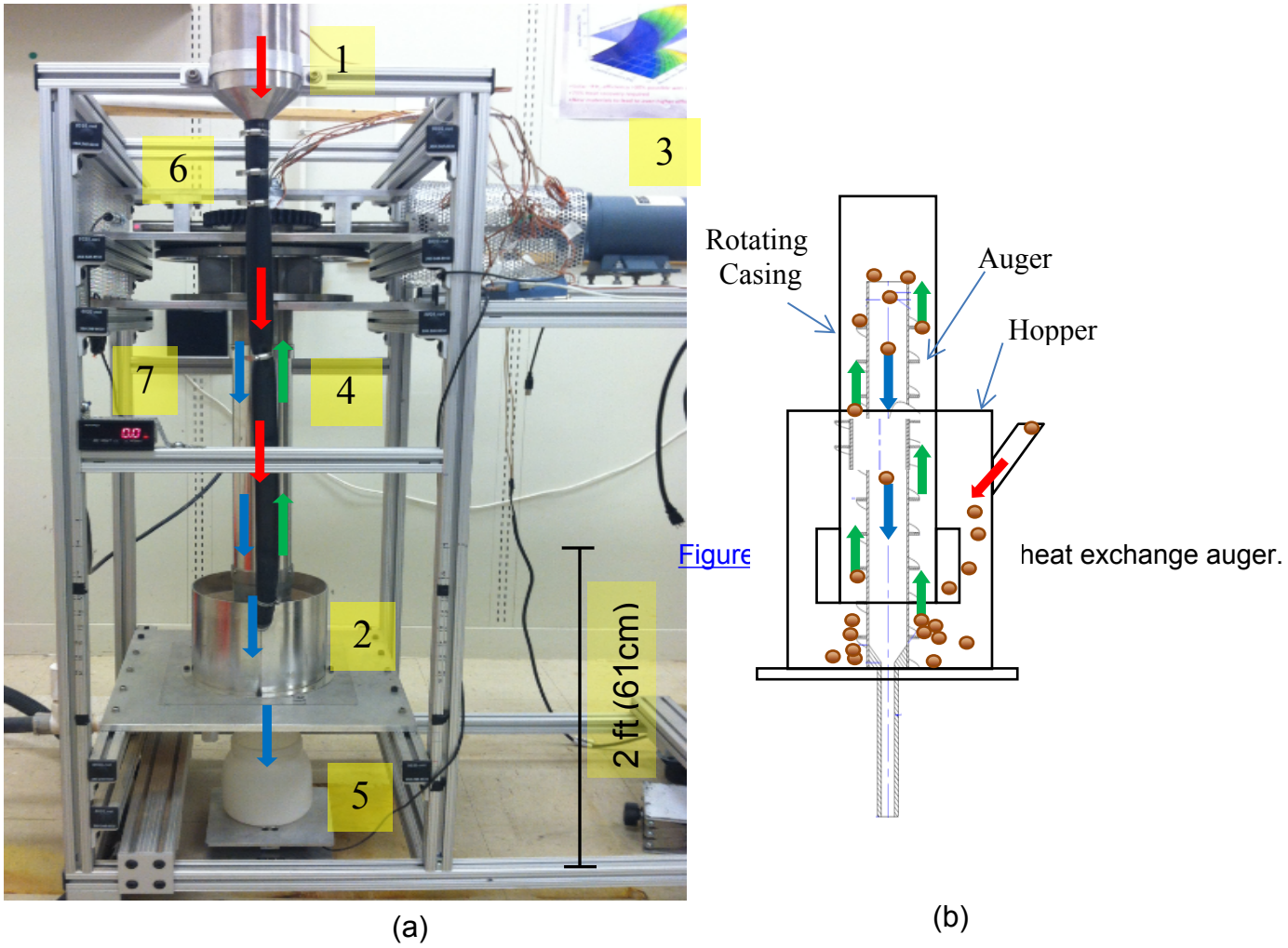

Figure 3. (a) Image of the PE. Sand is fed into the funnel (1) where it flows (red arrows) into the hopper (2). The motor (3) rotates the casing (4) conveying sand up the auger (green arrows). The downward flow (blue arrows) of sand was captured by a container resting on top of a scale (5). The driveshaft angular velocity was measured using an ROS (6) connected to a tachometer panel (7) to record the reading. (b) A cross section of the conveying pattern color coded to match the flow in (a).

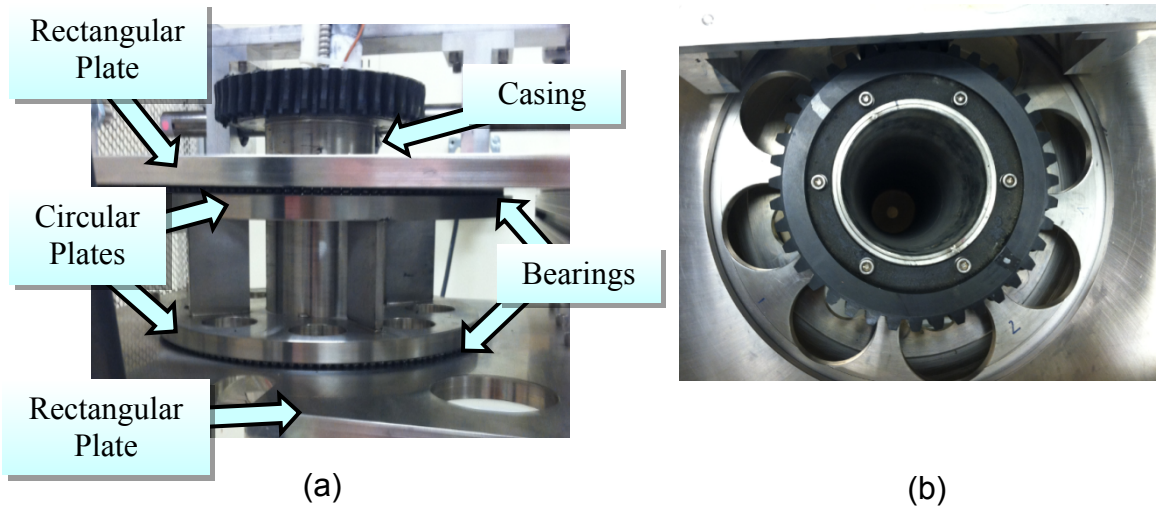

Figure 4. (a) Bearings are in grooves in the stationary (rectangular) plates, and rotating (cylindrical) plates. The casing is welded to the rotating plates. (b) A worm gear system with a reduction ratio of 1:40 was used to rotate the casing.

adjustable and was used to vary the sand level in the hopper. The sand level (or bed depth) was defined as the height between the hopper sand inlet and the top of the cutter (Figure 2). After the sand is conveyed and reaches the top of the auger, it flows down and out into a container placed under the PE at the auger shaft outlet (5 in Figure 3a).

The bed depth, casing angular velocity, and conveying rate were measured and recorded for all experiments. The casing angular velocity was measured using a Remote Optical Sensor (ROS). The sensor was optically aligned to illuminate a target of reflective tape on the driveshaft (6 in Figure 3a, Figure 5). A tachometer panel displayed the ROS output (7 in Figure 3a) which was scaled using the 1:40 worm gear ratio to calculate the casing angular velocity.

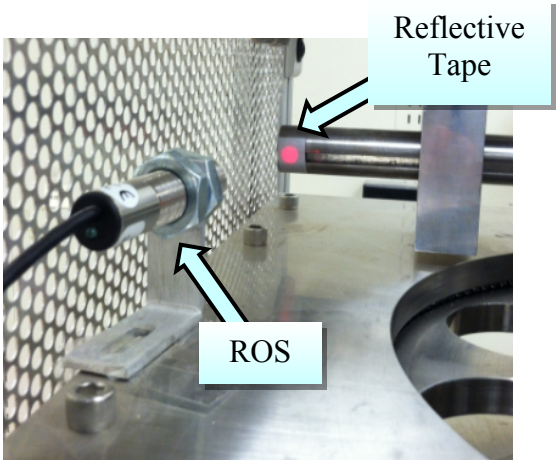

Figure 5. An ROS sensor directed at a target of reflective tape was used to measure the driveshaft angular velocity.

Conveying rate measurement preparation included filling the funnel to the brim and positioning the motor speed controller to a specific setting. Under the PE, a container was placed on top of a Loadstar 8 in. X 8 in. iWeigh digital scale to collect the downward flow of sand (5 in Figure 3a) and the scale output was logged by a computer. Experiments ran for a minimum of ten minutes and were repeated approximately 3-5 times for the same motor speed controller setting.

2. CONVEYING EFFICIENCY

2.1. Introduction

This section describes the evaluation of multiple auger designs, with the primary purpose of identifying a one that is compatible with efficient material conveying (~25%), and with heat recovery between particle flows. Typical augers have a single flight, with a pitch identical to the diameter. Furthermore, to maximize the conveying rate, auger shafts usually have a relatively small diameter compared to the diameter of the auger itself. Understanding that the thermal conductivity of particle beds is rather low, we evaluated auger designs that are characterized by low heat transfer distances in the beds. This approach aims to minimize the effect of the low thermal conductivity of packed beds and maximize heat transfer through the stainless steel body of the augers. Minimization of heat transfer distances was accomplished by two main design features. First, the use of multiple flights of the same pitch, with azimuthally offset starting locations. This arrangement decreases the vertical distance between neighboring flights (Figure 6). The second design feature was the use of a comparatively thick shaft, minimizing the radial thickness of the upward particle flow (Figure 6).

2.2. Experimental

2.2.1. Design and Setup

All auger prototypes were designed with the same overall dimensions but differed in the number of flights and single flight pitch. Table 1 lists the parameters used to characterize the designs, where A_N corresponds to the auger with N flights and single flight pitch, P. The A_2 and A_4 augers were designed with an identical single flight pitch but different flight number and similarly for A_3 and A_6. This approach was used to explore the dependence of the conveying rate on the number of flights, reflected in the decreasing vertical interflight distance—a desirable heat transfer property, but of uncertain effect on conveying rates. In addition, the pitch difference between the designs is used to find the dependence of the conveying rate on the pitch, specifically reflected in the slope of the flight. A longer pitch increases the theoretical capacity per revolution (equation (3)), but it also may suffer from poor efficiency as it requires conveying up a steeper flight slope. A schematic of the augers describing the parameters listed in Table 1 are shown in Figure 6. As shown in the figure, adding flights to the augers decreases the spacing between the flights and increases the auger's surface area.

Table 1. Auger Parameters

Auger, A_N	Number of Flights, N	Pitch, P [cm]	Auger Diameter, D [cm]	Flight thickness, T [cm]	Shaft O.D. [cm]
A_2	2	5.4	7.62	0.4	5.1
A_3	3	8.9	7.62	0.4	5.1
A_4	4	5.4	7.62	0.2	5.1
A_6	6	8.9	7.62	0.2	5.1

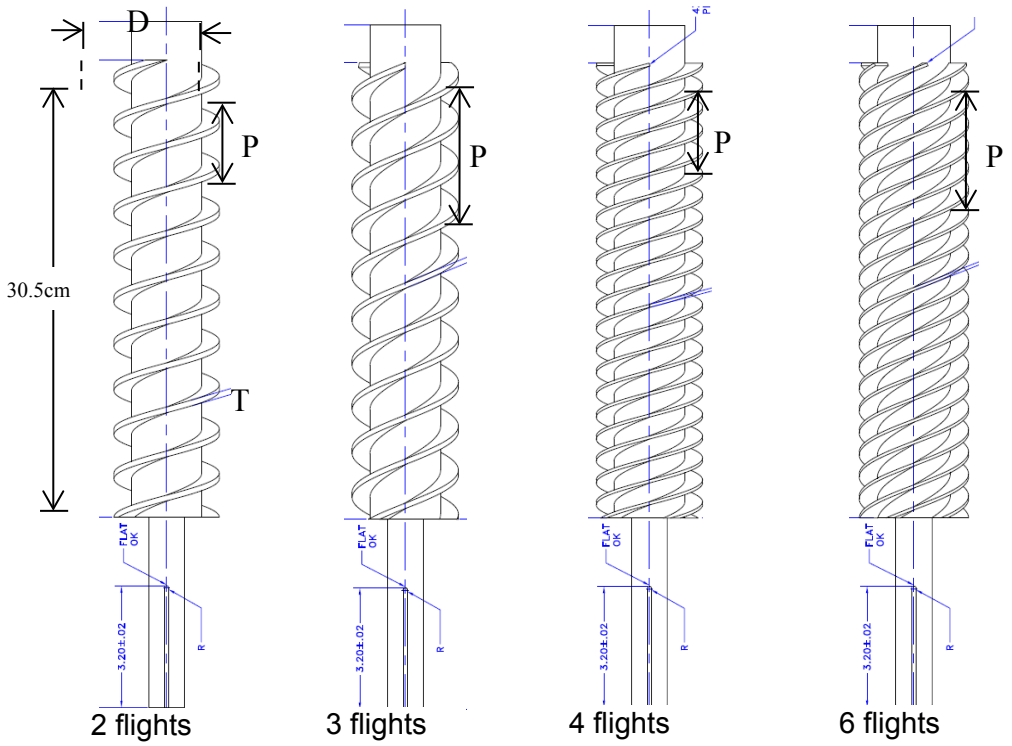

Figure 6. Diagrams of the four augers evaluated are shown above. P is the single flight pitch, D is the diameter, and T is the flight thickness. All augers have the same length of 30.5cm.

A conventional cutter (Figure 7), consisting of a design typical of Olds elevators, was used to sweep sand into the casing. The design consists of two protruding cutters ~5cm long, an inner diameter of 9.5cm, an outer diameter of 12.7cm, and a maximum gap of ~2cm.

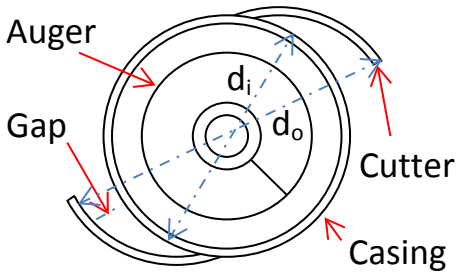

Figure 7. Top view of a conventional cutter, which consists of protruding cutters that sweep the sand into the conveyer. In the diagram, and correspond to the inner and outer diameters, respectively.

2.2.2. Measurements and Methods

The conveying rates of the four multi-flight augers were measured at 6 bed depths, between ~3cm and ~16cm. The measured conveying rate was used to calculate the conveying efficiency which is defined as the following ratio:

$$\eta = \frac{C_a}{C_{max}} \qquad (1)$$

Here, C_a is the measured conveying rate normalized to the casing angular velocity and C_{max} is the theoretical maximum conveying rate normalized to the casing angular velocity. Both quantities were normalized to directly calculate the efficiency with the values measured in the experiments. The maximum conveying rate is calculated by using the smaller of either the theoretical volume swept by the cutters, V_c, or the theoretical volume conveyed along the casing axis of rotation, V_a, which is known as the theoretical volumetric capacity. The smaller of the two values sets a limit on the maximum amount of material that can be conveyed. The theoretical volume swept by the cutters per revolution is given by:

$$V_c = \frac{\pi}{4}\left(d_o{}^2 - d_i{}^2\right)H \qquad (2)$$

where d_o, is the outer cutter diameter, d_i is the inner cutter diameter, and H is the cutter height. Similarly, the theoretical volumetric capacity per revolution is given by:

$$V_a = \frac{\pi}{4}\left(d_{casing}{}^2 - d_{shaft}{}^2\right)P \qquad (3)$$

where d_{casing}, is the inner casing diameter, d_{shaft} is the outer auger shaft diameter, and P is the auger single flight pitch. Equation (3) can be used to calculate C_{max} if the auger flight volume is negligible when compared to V_a. As is evident in Figure 6, the flights of the augers evaluated in this project are not negligibly thin, when compared to the effective pitch (individual pitch, divided by the number of flights). To account for the finite flight volume, the auger flight volume for one revolution of the flight was calculated (i.e., the volume of the flight that traverses a height equal to its pitch) using the formula for the surface area of a helicoid with inner and outer diameters equal to the corresponding auger's flight dimensions and multiplying it by the flight thickness:

$$V_{flight} = \frac{\pi\, T}{4}\left[d_2\left(d_2{}^2 + 4P^2\right)^{\frac{1}{2}} - d_1\left(d_1{}^2 + 4P^2\right)^{\frac{1}{2}} + 4P^2 ln\left(\frac{\left(d_2{}^2 + 4P^2\right)^{\frac{1}{2}} + d_2}{\left(d_1{}^2 + 4P^2\right)^{\frac{1}{2}} + d_1}\right)\right]_{r_0} \qquad (4)$$

where d_2, is the auger diameter, d_1 is the auger shaft outer diameter, P is the auger single flight pitch, and T is the flight thickness (provided in Table 1 for each auger). V_{flight} was then multiplied by the corresponding number of flights, and showed that the auger flights occupied a volume ~17%-25% of V_a and is not negligible.

Taking the auger flight volume into account modifies the volumetric theoretical capacity to:

$$V_{mod} = V_a - V_{flight} \quad (5)$$

V_{mod} will be referred to as the modified theoretical volumetric capacity and, when considering the auger flight volume, is used to calculate C_{max}. The theoretical conveying rates were calculated by multiplying V_{mod} and V_c by the silica sand bulk density, ρ (measured to be 1.51g/cm^3). Some of the calculated values are given in Table 2 for comparison. CNC in Table 2 represents the conventional cutter and ZPC represents a zero-profile cutter which is discussed in section 3.

Table 2. Theoretical Conveying Rates and Capacities

Auger, A_N	**Theoretical Volumetric Capacity per revolution [cm³], V_a**	**Modified Theoretical Volumetric Capacity per revolution [cm³], V_{mod}**	**Theoretical Conveying Rate [(g/s)/rpm], $\left(C_{max} = {\rho V_{mod}}/{60}\right)$**
A_2	245.8	203	5.11
A_3	368.7	279.1	7.02
A_4	245.8	203	5.11
A_6	368.7	279.6	7.04
Cutter Design	**Theoretical Volume Swept by the Cutters per revolution [cm³], V_c**		**Theoretical Conveying Rate [(g/s)/rpm], $\left(C_{max} = {\rho V_c}/{60}\right)$**
CNC	285.7		7.19
ZPC	96.5		2.43

2.3. Results and Discussion

Figure 8 shows plots of the conveying rate as a function of casing angular velocity for the A_2, A_3, and A_4 augers. The bed depth at which the conveying rate measurements were taken is given at the top of each plot. Data points distributed around a particular conveying rate and casing angular velocity represent multiple experiments at the same nominal motor speed control setting. All plots exhibit a linear relationship between the conveying rate and casing angular velocity for all augers, which agrees with the literature on the Olds Elevator.[4] The slopes of the conveying rate linear fits are shown so that conveying rates of different augers at different bed depths can be easily compared. The consistent small negative 0^{th} order coefficients for all augers and experimental conditions imply that a small but finite casing angular velocity is required to initiate conveying. The slope of the conveying rates represents the increase in conveying rate per increase in casing angular velocity. Alternatively, the slope can be seen as the conveying rate normalized to the casing angular velocity (C_{norm}). Owing to high mechanical resistance, casing rotation was not achieved for any bed depth for auger A_6, and conveying rates could not be measured. Similarly casing rotation was achieved only for one bed depth for the A_4 auger (Figure 8a). Comparing C_{norm} in each of the four plots shows that the A_2 auger conveying rate was higher than that produced by all other augers for all angular velocities and bed depths. The A_3 auger conveyed less than the A_2 auger, however, the difference in C_{norm} decreased as the bed depth

increased. This decrease can be seen more clearly in Figure 9 which shows a plot of C_{norm} as a function of bed depth for the A_2, A_3, and A_4 augers.

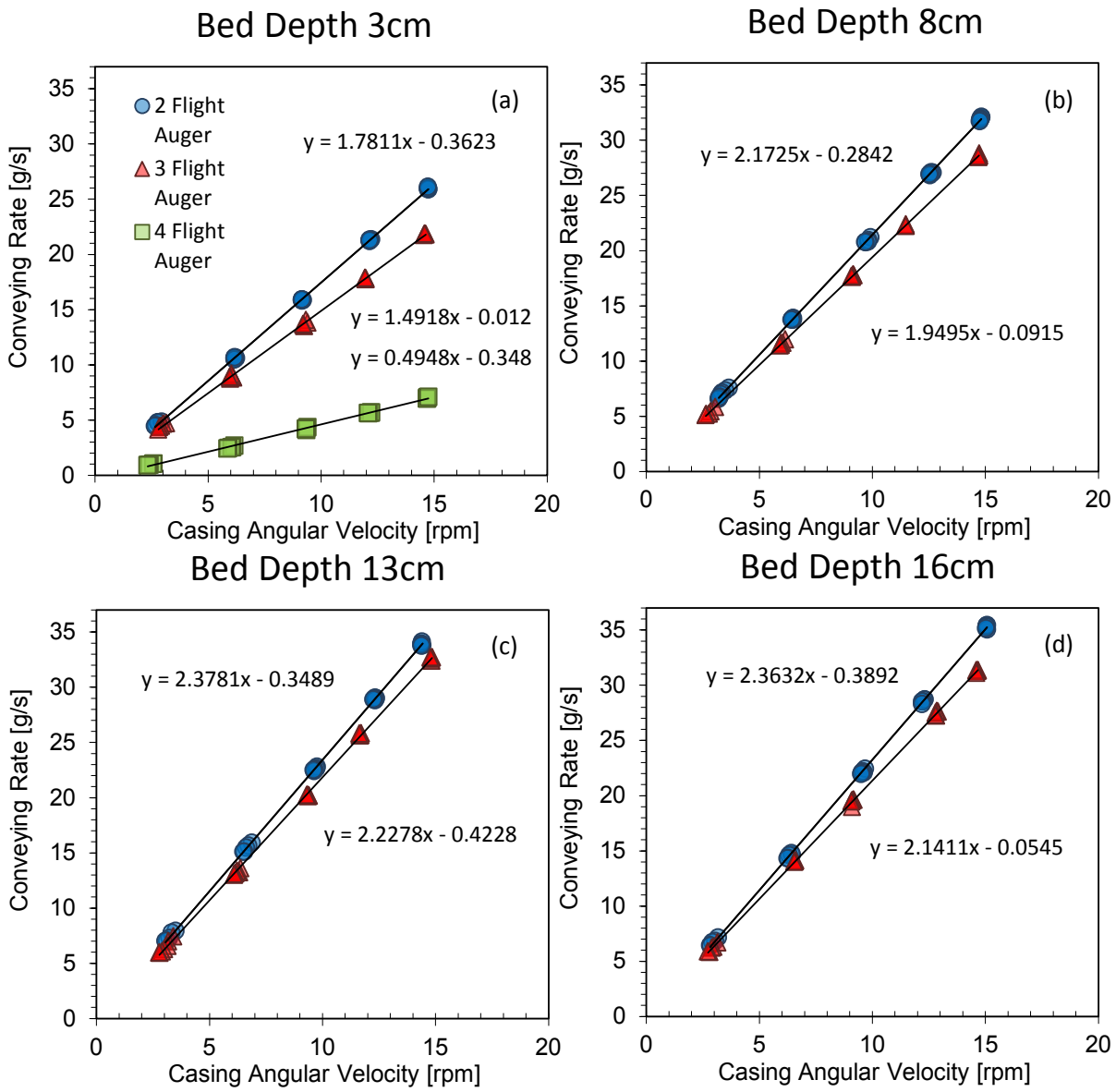

Figure 8. Conveying rate as a function of casing angular velocity for the A_2, A_3, and A_4 augers for four bed depths. The A_4 auger conveyed sand for only one bed depth (a). At other bed depths, it increased counter torque and casing rotation was not achieved. Similarly, the counter torque produced when using the A_6 auger did not allow casing rotation for any bed depths.

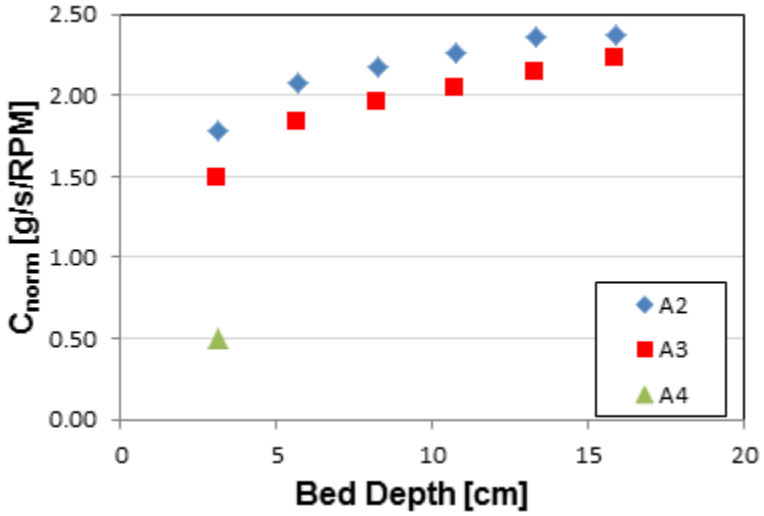

Figure 9. Normalized conveying rate as a function bed depth for the A_2, A_3, and A_4 augers. The A_4 auger conveyed sand for only one bed depth because, due to an increase in counter torque, casing rotation was not achieved for all other bed depths.

Conveying Efficiency

Figure 10 shows the average conveying efficiency as a function of bed depth for the A_2, A_3, and A_4 augers. The data points are results from calculations performed using equation (1) where equation (5) was used to calculate C_{max} because the modified theoretical capacity limits the maximum amount of material that can be conveyed (see section 2). C_a was calculated by taking the measured conveying rates for each experiment and normalizing them to the casing angular velocity in rpm. The data points in the plot are C_a calculations averaged for the same casing angular velocity. The shape of the conveying efficiency curve is similar to the curve in Figure 9; however, the conveying efficiency curves are farther apart. The divergence between the curves is

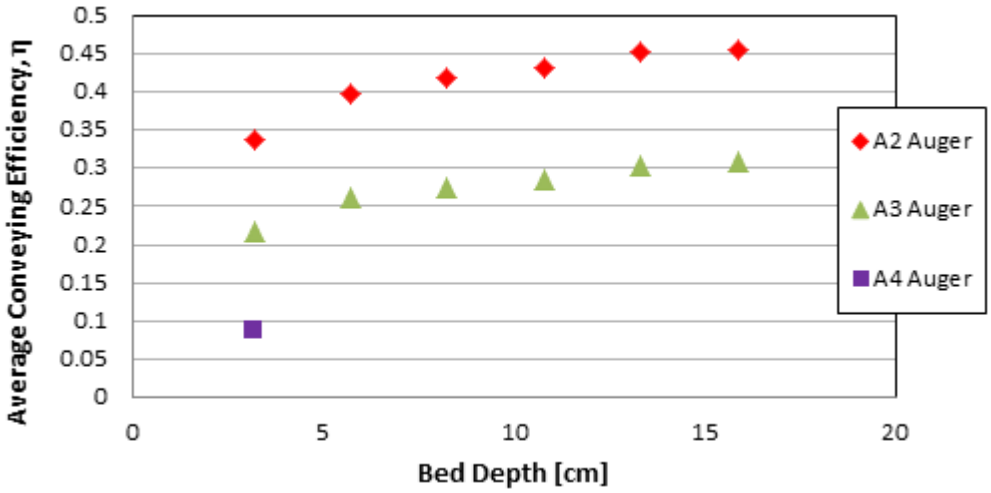

Figure 10. Conveying efficiency as a function of bed depth for the A_2, A_3, and A_4 augers.

due to the A_3 auger having a greater theoretical volumetric capacity than the A_2 auger. This difference results in a greater C_{max} and, in conjunction with the lower conveying rate produced by the A_3 auger (when compared to the A_2 auger), lowers the relative conveying efficiency for the A_3 auger. For bed depths greater than ~14cm the slope of the efficiency curves level out for both augers. This behavior indicates an upper bound on the conveying efficiency for the A_3 auger of $\eta \approx 45\%$ and $\eta \approx 32\%$ for the A_2 auger.

Depending on the desired conveying efficiency, a compromise design probably exists between the A_2 and A_4 augers, such that it exhibits an acceptable conveying characteristic, while decreasing the flight spacing with respect to A_2, and likely improving heat transfer.

The influence of the bed depth on the conveying rates and efficiencies indicates that the sweeping action of the cutters is not the sole mechanism for feeding material into the elevator, and that a horizontal component of the solids pressure also plays a role. This effect is exploited in the experiments described in the following section, to evaluate the feasibility of using zero-profile cutters.

3. CUTTER DESIGN

3.1. Introduction

This section describes the evaluation of a zero-profile cutter (Figure 11). The zero-profile cutter (ZPC) provides adequate room for a tightly nested auger system which would be necessary for the PE to be scalable. The ZPC design also reduces the risk of fractures that may result from structural weak points such as the cutter/casing joint in the conventional cutter (CNC). Fractures on the cutter/casing joint in the CNC may arise due to forces acting on the cutter while sweeping the material into the casing. These forces can be quite substantial, as evidenced by the inability to rotate the casing with some of the augers (see section 2.3). To test and compare the conveying properties of the CNC and the ZPC, a series of identical conveying experiments were performed for each. With this information, the conveying rate for each design was used to determine the effectiveness of the ZPC.

3.2. Experimental

3.2.1. Design and Setup

The ZPC was designed with rigid tapered edges in place of protruding cutters that are used in the conventional cutter design (Figure 7). While the CNC is designed with protruding cutters to sweep sand into the elevator, the ZPC relies more heavily on the horizontal component of the solids pressure to feed sand into the elevator. The greater dependence of the ZPC on horizontal pressure is due to the finite and thin profile of its cutters, which is dictated by the material thickness. To increase the sand intake of the ZPC, it was designed with four cutouts (Figure 11).

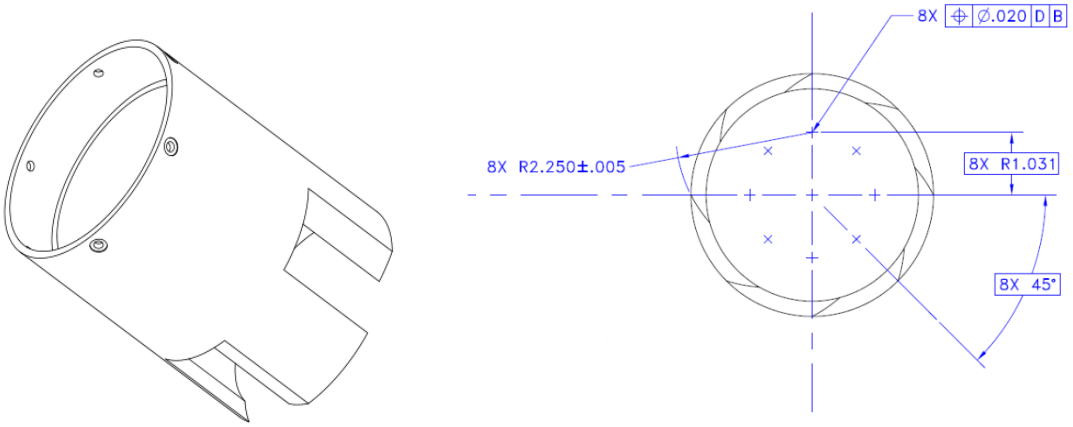

Figure 11. (a) The zero-profile cutter design consists of four cutouts with sharp tapered edges that sweep particles into the conveyor. (b) A schematic showing the dimensions of the four cutouts and the curvature of the tapered edges.

3.3. Results and Discussion

The Conveying Rate as a Function of Casing Angular Velocity

To measure the conveying rate using the ZPC, the A_2 and A_3 augers were used. Figure 12 and Figure 13 show the conveying rate as a function of casing angular velocity. The data points are measurements from identical experiments conducted using the CNC and ZPC. Each graph shows data taken at a particular bed depth for the various auger casing combinations. As can be seen in all figures, C_{norm} (the slope of the linear fits) is greater when using the CNC than when using the ZPC for all bed depths, signifying a greater conveying rate. Additionally, the difference in C_{norm} between the different augers is much greater when using the ZPC than when using the CNC. This behavior signifies that the auger geometry has a greater impact on the conveying rate for the ZPC than for the CNC. Overall, the CNC conveys more per unit time at lower casing angular velocities than the ZPC. For instance, at a bed depth of 10.8cm the {A_2, CNC} combination produced a C_{norm} of ~2.3g/s/rpm which is ~140% greater than the {A_2, ZPC} combination. Similarly, {A_3, CNC} produced a C_{norm} 370% greater than the {A_3, ZPC} combination for the same bed depth. Although the CNC has a greater conveying rate per unit time, the impact of the auger geometry on the ZPC shows that a nested auger system is feasible and its conveying rate can be maximized by choosing an auger with the optimal geometry.

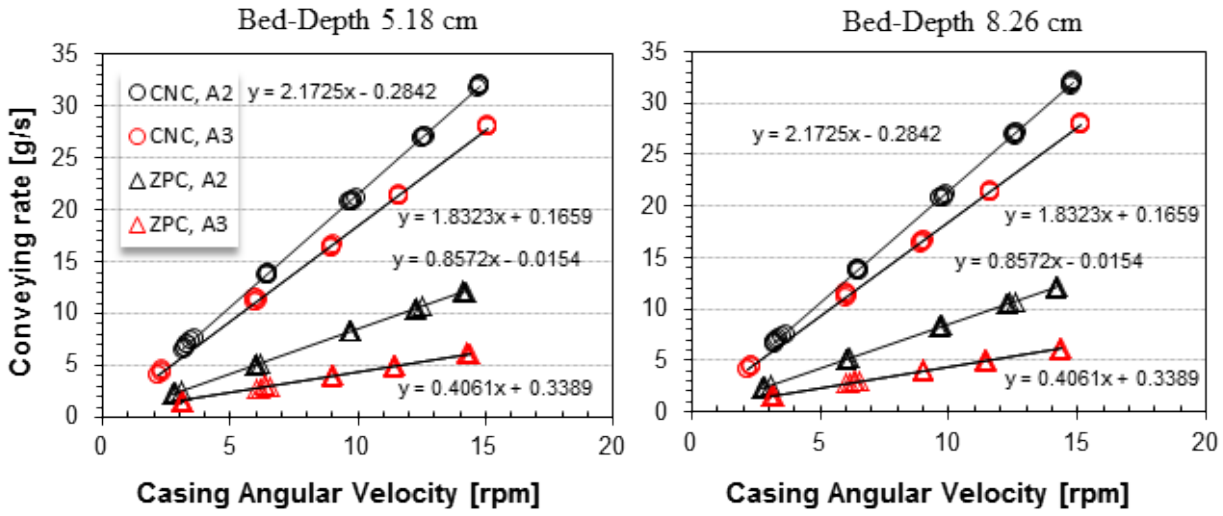

Figure 12. Conveying rate as a function of casing angular velocity is shown above for experiments conducted using the CNC and ZPC with the A_2 (2-flight) and A_3 (3-flight) augers. The conveying rate measurements were taken at a bed depth indicated at the top of each plot.

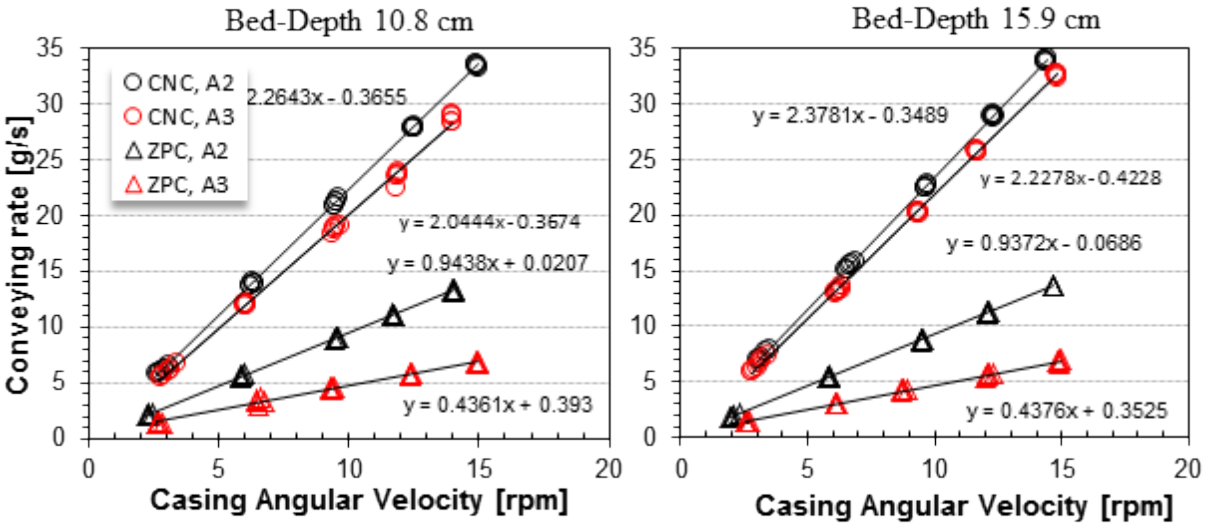

Figure 13. Conveying rate as a function of casing angular velocity is shown above for experiments conducted using the CNC and ZPC with the A_2 (2-flight) and A_3 (3-flight) augers. The conveying rate measurements were taken at a bed depth indicated at the top of each plot.

Normalized Conveying Rate as a Function of Bed Depth

Figure 14 shows C_{norm} as a function of bed depth for the experiments discussed above. All the curves have the same general shape; a steeper slope for shallow bed depths which becomes less steep as the bed depth increases. The CNC has a 300% - 140% greater C_{norm} than the ZPC for all bed depths. In addition, the slope of the curves for the ZPC become slightly negative for the

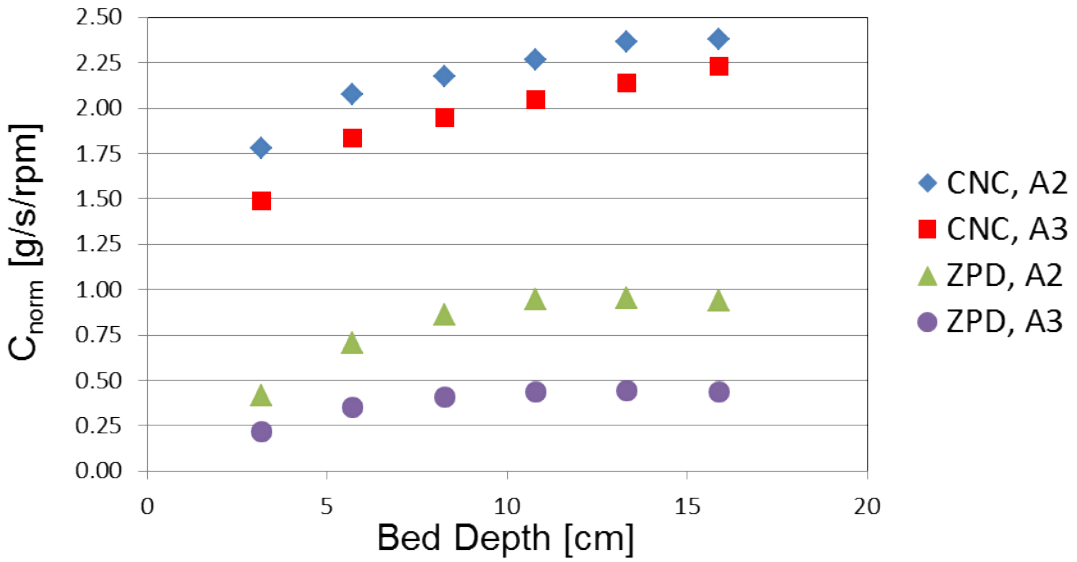

Figure 14. The slope of the normalized conveying rate curve for both cutter designs is positive for shallow bed depths; however, the slope for the CNC curve levels out as the bed depth increases while becoming negative for the ZPC after a characteristic bed depth.

greatest bed depths considered signifying that increasing the bed depth will not increase its conveying efficiency.
Although the conveying rate is not as high as the CNC, using a ZPC is feasible, and tightly nested elevators can be constructed, to enable a capacity scaling with the square of the heat exchanger diameter. It is important to note that the evaluated ZPC design was deliberately thin, and that in practice a design falling between the ZPC and CNC would likely be used.

The Conveying Efficiency of the ZPC

Figure 15 shows the conveying efficiency as a function of bed depth using the ZPC in combination with the A_2 and A_3 augers. The data points are results from calculations using equation (1), where V_c was used for C_{max} and its value was obtained from Table 2. The initial difference in conveying efficiency between the two augers is relatively small and increases substantially as the bed depth increases. The efficiency reaches a maximum at ~11cm for the A_2 auger and ~12cm for the A_3 auger. After this maximum, the efficiency begins to decrease for both augers implying that there is a bed depth that will optimize the conveying efficiency. The figure also shows that the A_2 auger conveyed a maximum of ~20% more than the A_3 auger when used in combination with the ZPC. This result is in agreement with previous results that state the auger geometry has a substantial effect on the conveying rate of the PE when using the ZPC. Although the ZPC does not convey as much as the CNC per unit time, there appears to be an optimal auger/cutter combination that maximizes the conveying efficiency when using the ZPC.

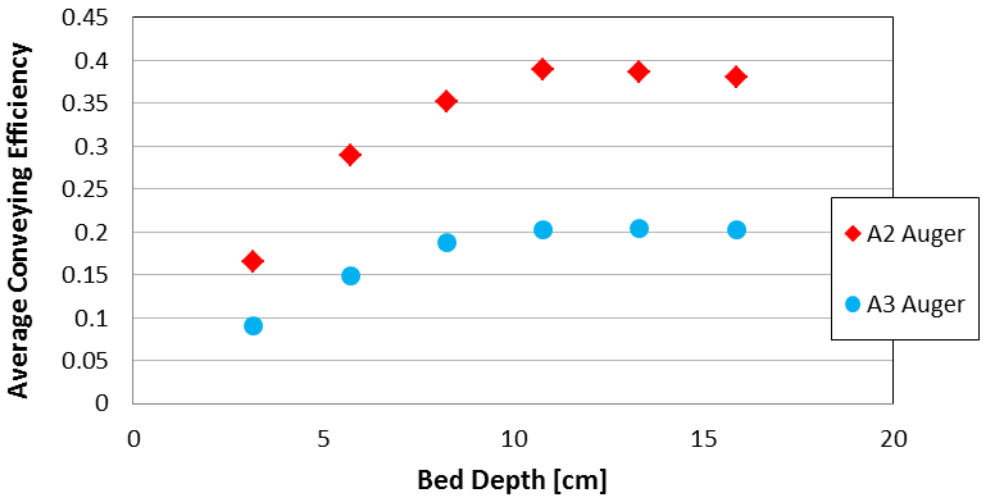

Figure 15. The conveying efficiency as a function of bed depth when using the ZPC with the A_2 and A_3 augers. The above data was calculated using equation (1) where was calculated by considering the maximum volume swept by the ZPC cutters, , whose value is given in Table 2

4. TWO CONCENTRIC ELEVATORS

4.1. Introduction

This section describes the design and evaluation of a PE with two concentric auger/casing pairs, the so-called nested auger system. A nested auger system is needed to achieve the volume scalability of the PE. In addition, by preserving the conveying pattern of the single auger PE between nested augers radial heat exchange between multiple concentric particle flows is made possible. As is shown in Figure 16, the flow pattern was designed so that counter-current particle flows are separated by either an auger or the cylindrical wall of a casing. This arrangement would make the auger and casing wall the mediums through which heat transfer would occur. To demonstrate the feasibility of a nested auger particle elevator, a prototype was constructed and its conveying rate was measured verifying the full functionality of the system.

4.2. Experimental

4.2.1. Design and Setup

Figure 17 shows a model displaying the internal components of the nested auger system. Using the existing PE, two augers were concentrically installed on two parallel stainless steel plates. The inner elevator consists of an A_2 auger and a 9.5cm O.D. casing that are concentrically placed down the inner shaft of the outer elevator. The outer elevator consists of an A_2 auger and a 9.5cm O.D. casing that are concentrically placed down the inner shaft of the outer elevator. The outer elevator consists of a 30.5cm long single flight auger with a flight width of 1.3cm and 10.2cm

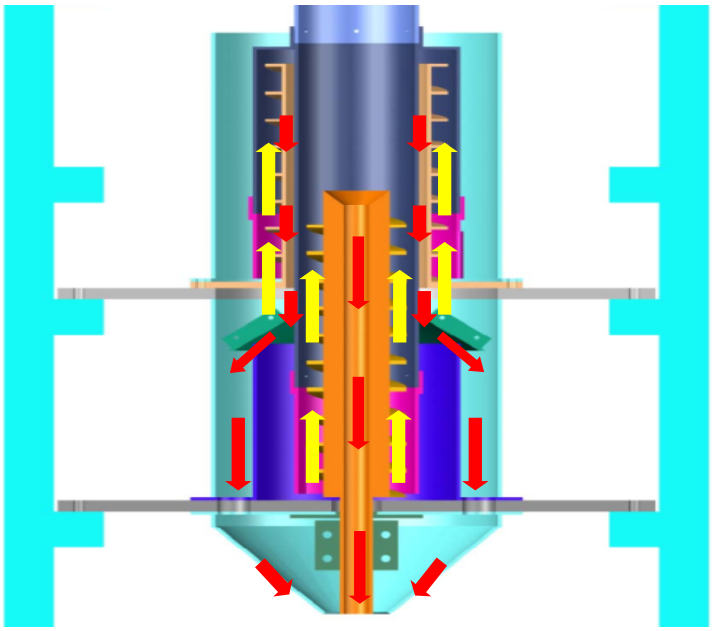

Figure 16. The above cross section depicts the sand flow inside the nested auger system. The concentric casings rotate simultaneously driving sand up their respective augers (yellow arrows). The sand flows down and out the system (red arrows) after reaching the top of the auger.

pitch. The outer auger shaft was made with a 10.8cm inner diameter to provide enough clearance for the inner auger casing to rotate. The outer casing has an inner diameter of 15.2cm. Due to their high conveying efficiency, CNC cutters were used to sweep sand into both elevators. The inner auger bed depth was 5.7cm and the outer auger bed depth was 7.6cm. A series of holes were bored into the lower plate in a circular pattern which had a diameter slightly larger than the inner hopper diameter to allow sand to flow down and out into a container. A guide was used to combine both downward flows of sand underneath the device where it was collected using a container resting on top of a digital scale.

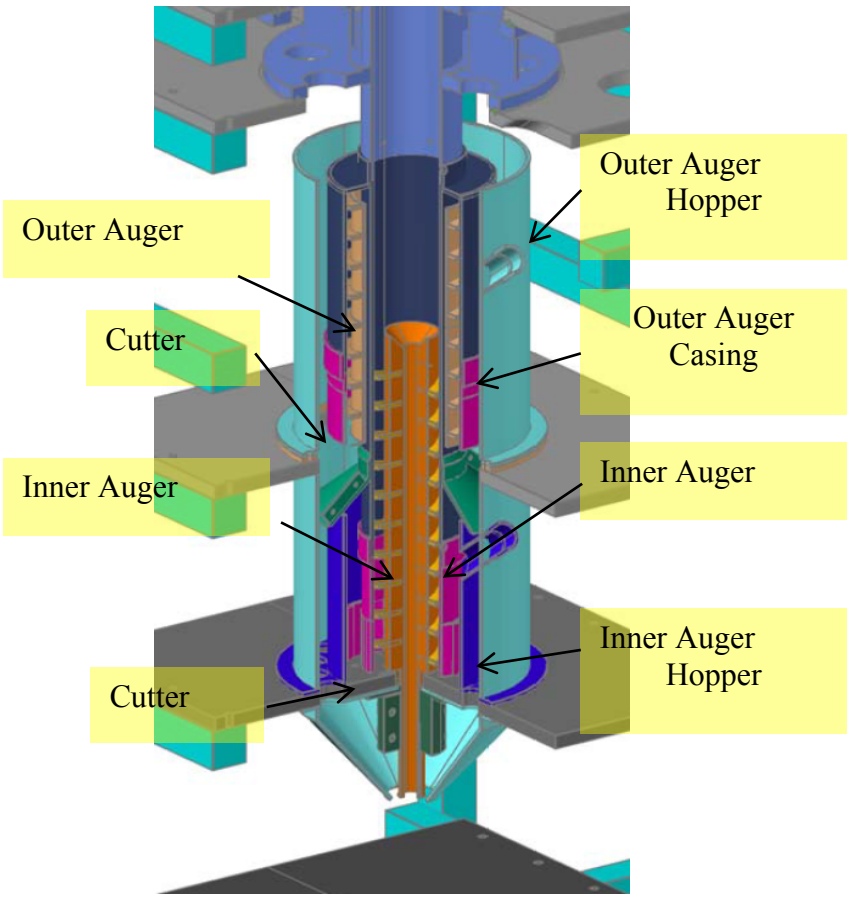

Figure 17. The above is a 3-d model of the nested auger system. The parts are color coded: pink - CNC cutters; dark blue – rotating casings; turquoise – outer hopper; blue – inner hopper.

4.3. Results and Discussion

The conveying rate as a function of casing angular velocity is shown in Figure 18. The nested auger system preserves the linearity between the conveying rate and casing angular velocity which enables precise sand volumetric flow control. To compare the conveying effectiveness of the nested system, its conveying results were compared with the results of the A_2 single auger system, which had the greatest conveying rate when using a single auger. The A_2 conveyed a maximum of ~34g/s at ~14rpm and a bed depth of 13.3cm (section 2). In contrast, the nested auger system conveyed a maximum of ~50g/s at ~7rpm. In addition to providing a conveying pattern that could be used to exchange heat between concentric particle flows, the nested auger

elevator produced a conveying rate greater than the most efficient single auger system evaluated in this report at a lower casing angular velocity.

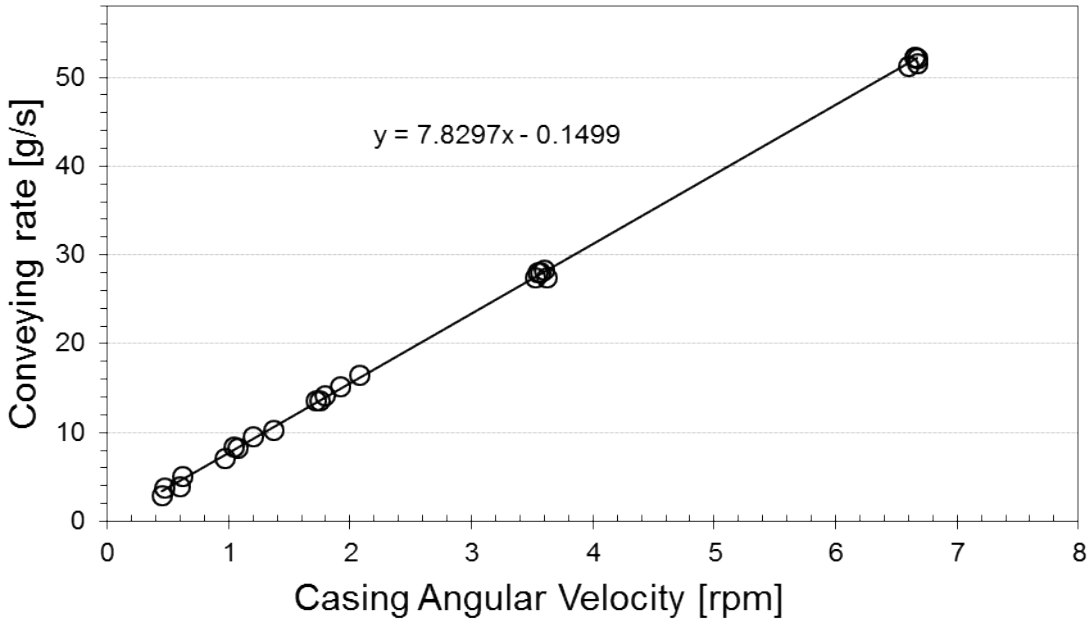

Figure 18. The above plot shows the conveying rate as a function of casing angular velocity for the compound PE.

5. HEAT RECOVERY

5.1. Introduction

In this section, heat exchange between counter-current particle flows is evaluated using a single auger elevator. The conveying pattern of the PE is exploited to transfer heat from a heated bed flowing down through the auger's hollow shaft to room temperature sand conveyed up the auger flights (Figure 19). Because the auger is the medium through which heat transfer occurs, its design and geometry are important for effective heat exchange between particle flows. For this reason a new auger was designed with a thin shaft wall to increase heat transfer through the auger. In addition the auger characteristics that produced the greatest conveying rate in section 2 were implemented to maximize the conveying efficiency. The heat exchange power and heat recovery were measured to quantify the effectiveness of the design. The experimental design, setup, and measurement methods are discussed in section 5.2 and section 5.3 presents the results.

5.2. Experimental

5.2.1. Design and Setup

The experiments were conducted with a single auger system. The auger was designed with 2-flights, a single flight pitch of 5.4cm, and an outer diameter of 5cm. To increase heat exchange the design included thinner walls and flights (both 2mm thick) and a total length of 70cm. The thin walls minimize thermal resistance and the increase in length (compared to the augers used in

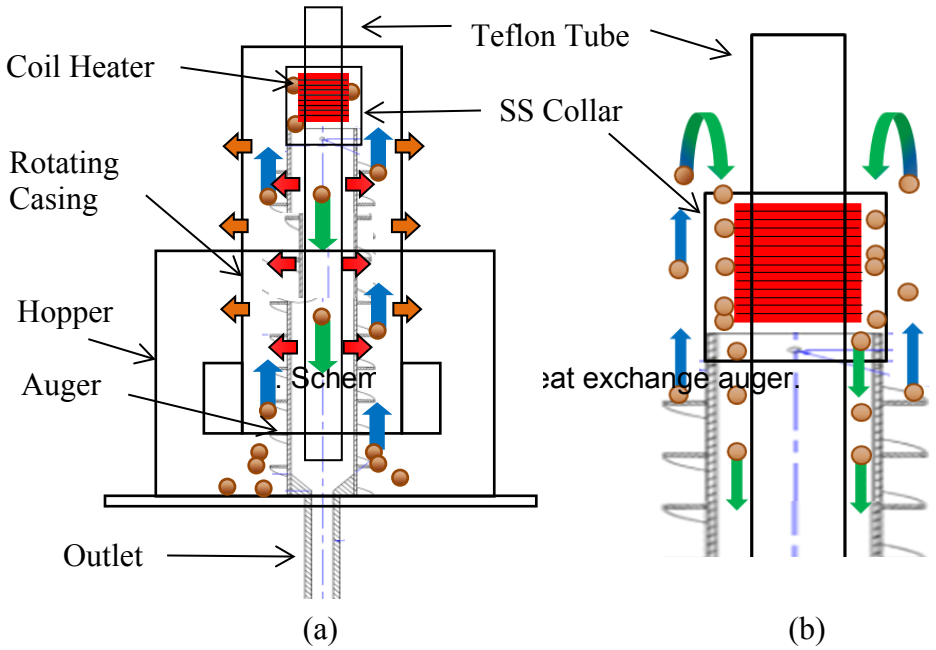

Figure 19. (a) The coil heater heats the sand flowing downward (green arrows) and heat is radially transferred to the cool sand conveyed up the auger (green arrows). (b) A closer look at the heater shows how the sand was localized into close contact with the heater. Only a few particles are shown for clarity.

section 2) allows additional time for heat transfer between the particle flows. Lastly, due to its high conveying capacity the conventional cutter design was used to sweep sand into the casing.

To test heat recovery between the particle flows, room temperature sand was conveyed to the top of the auger where it was heated by a coil before flowing down the hollow auger shaft (Figure

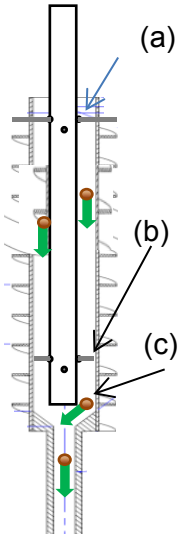

eat exchange auger.

Figure 20. The cross section above shows how SS pins were used: (a) to hold the Teflon tube in place, SS pins were slipped through holes bored into the auger shaft wall and the Teflon tube. (b) SS pins were also used to center the Teflon tube in the auger shaft. (c) A gap between the Teflon tube and bottom of the auger allows sand to flow out through the bottom of the auger.

19). To reduce sand volume at the center of the auger shaft (that would be otherwise unused in heat transfer), a 3.2cm O.D. Teflon tube was concentrically placed down the shaft center (Figure 20, A in Figure 21). The Teflon tube also reduces heat loss through the center of the auger shaft by reducing the effective heat transfer area between the air and sand to an annulus (less area). The tube was held in place by two stainless steel (SS) pins cut slightly longer than the auger shaft O.D. that slid into two sets of offset holes bored 1cm and 1.7cm down from the top of the auger ((a) in Figure 20). The pins held the Teflon tube 2.5cm above the hopper plate ((c) Figure 20),

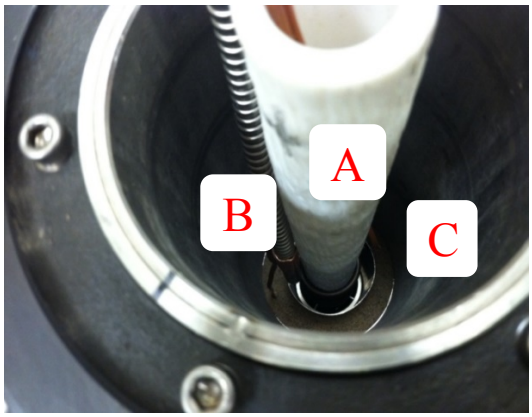

Figure 21. Looking down the center of the worm gear of the particle elevator: A. Teflon tube, B. heating coil, C. stainless steel collar.

leaving a gap to allow the downward sand flow to exit into a container. In addition, SS pins cut to a length slightly shorter than the I.D. of the auger shaft were slipped into holes bored into the Teflon tube as needed to center it in the auger shaft ((b) Figure 20).

Figure 22. The coil heater used to heat the sand.

A 900 Watt/120 V coil heater was designed and custom built to heat the sand (Figure 22**)**. The coil heater was designed with a 3.8cm O.D., 3.2cm I.D., and 7.6cm width. The heater was slipped over the Teflon tube to a distance ~1.3cm above the top of the auger (B in Figure 21). The Teflon tube O.D. was slightly larger than the coil heater I.D. and was shaved down to create a tight fit to hold the heater in place. A 12.7cm wide 304 SS steel collar (26 gauge) was cut and formed into a cylinder and slipped over the top of the auger (C in Figure 21) to localize the downward sand flow into close contact with the heater. The downward sand flow rate was controlled using a butterfly type valve which was slipped over the auger shaft outlet located underneath the PE.

The coil heater was equipped with a J-type thermocouple (TC) installed within its coils to measure its internal temperature. The coil heater voltage, V_{coil}, was varied using a 12A variable transformer. Three voltages settings were used (30V, 35V, and 50V) to change the temperature of the sand flowing downward, testing the heat recovery's dependence on temperature. To measure the sand temperature, electrically insulated J-type TCs were used.

Table 3. TC Placements

Symbol	Figure Letter	TC Placements
T_{TA} (Top of Auger)	(a)	3.2cm below the top of the auger
T_{TT} (Top of Teflon Tube)	(b)	Adjacent to (a) on the Teflon
T_{MA} (Middle of Auger)	(c)	30.5cm above the bottom of the auger
T_{MT} (Middle of Teflon Tube)	(d)	Adjacent to (c) on the Teflon
T_{BT} (Bottom of Teflon Tube)	(e)	2.54cm above the Teflon tube bottom

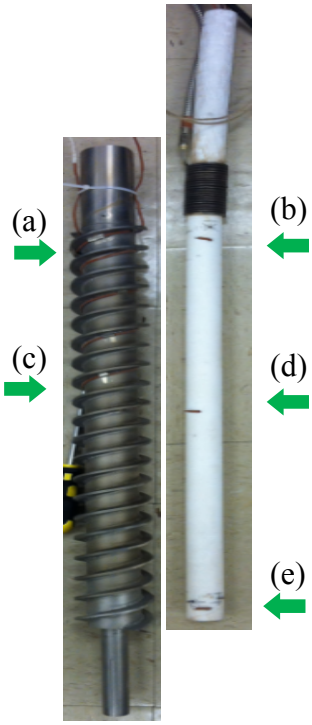

Figure 23. The TC placements on the auger and Teflon tube are indicated by the green arrows and are discussed in Table 3

The TCs were placed in five different locations (green arrows in Figure 23). A description of the TC placements is presented in Table 3 and the placements are show graphically in Figure 23 which also shows the relative scale of the auger and Teflon tube. The TCs were wrapped underneath the auger flights and around the auger shaft and were held in place by 304 stainless steel foil (33 gauge) spot welded to the auger shaft and flights (Figure 24).

Figure 24. The TCs were strapped to the auger by 304 stainless steel foil (33 gauge) spot welded to the auger shaft.

To reduce radial heat transfer to the surroundings, flexible fiberglass insulation (0.3cm thick, R- value of 0.1K m^2/W) was wrapped and secured around the casing. To test the effectiveness of the insulation, identical experiments were performed with 0, 3, and 6 layers of insulation.

5.2.2. Measurement and Methods

The TC temperature measurements were logged using an Omega OM-USB data acquisition device (DAQ). The DAQ data was plotted during each experiment using the TracerDAQ Strip Chart software provided with the DAQ. Data from both the digital scale and the DAQ were logged concurrently.

The heat exchange between particle flows in the PE was calculated using the following efficiency equations:

$$\varepsilon_R = \frac{T_{TA} - T}{T_{TT} - T}, \quad \varepsilon_L = \frac{(T_{TA} - T_F) - (T_{TT} - T_B}{T_{TT} - T_F}, \quad \varepsilon = \frac{T_{BT} - T_F}{T_{TT} - T_F}, \tag{6}$$

where ε_R is the heat recovery efficiency, ε_L is the heat loss fraction, and, ε is a measure of the non-ideality of the system. All the variables represent temperatures at different locations on the PE, specifically: TA ≡ Top of Auger, TT ≡ Top of Teflon, F ≡ Funnel, BT ≡ Bottom of Teflon (Table 3, Figure 23). The effective heat recovery, ε_R, is a measure of how much heat is transferred from the heated downward flow of sand to the cooler sand conveyed up the auger. The effective heat loss, ε_L, is a measure of how much heat was lost to the environment. The efficiency ε was introduced to characterize the non-ideal behavior of the heat exchanger. Ideally, the outlet temperature $T_{BT}=T_F$ for a countercurrent heat exchanger and thus $\varepsilon=0$. In practice, ε expresses the extent to which the PE can be considered an ideal heat exchanger.

In addition to the heat recovery effectiveness, the heat exchange power, P, was calculated. The heat exchange power indicates the amount of energy that is transferred from the hot downward flow of sand to the cool upward conveyed sand. The heat exchange power was calculated using:

$$P_{heat} = \dot{m}c(T_{TA} - T_F) \quad (7)$$

where $\dot{m}$ is the experimentally measured conveying rate and c is the specific heat capacity. The specific heat capacity for quartz sand (0.83J/g K) was used in the calculations.

5.3. Results and Discussion

The temperature measurements were logged using the DAQ and are shown in Figure 25. The results shown are for an experiment with the following settings: V_{coil}=50V, ω=3.4rpm, and 3 insulation layers. The top-most curve (red curve) is the temperature measurement of the sand flowing past the TC installed at the top-most position of the Teflon tube (b in Figure 23). As can be seen from the figure, the sand is heated from an average of 21ºC to 78ºC by the time it reaches the top of the auger. The corresponding heat recovery efficiency for this particular experiment, calculated using equation (6), is ε_R=45%. Similar plots were used to calculate the efficiencies using equation (6) and produce the plots in the following section.

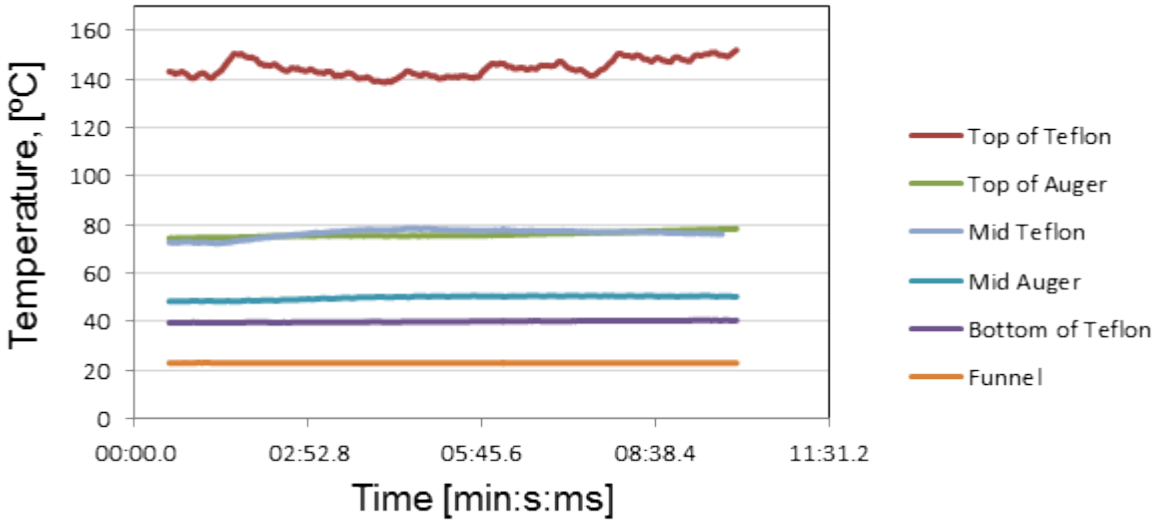

Figure 25. Plot of the temperature measurements taken as a function of time. The above results were measured for: V_{coil}=50V, ω=3.4 rpm, and 3 insulation layers.

5.3.1. Effective Heat Recovery

Figure 26 shows three plots of the heat recovery, ε_R, as a function of T_{TT} for three different layers of insulation wrapped around the casing. The different colors are used to represent data from experiments conducted at different casing angular velocities. The value of T_{TT} was changed by changing the voltage setting on the variable transformer. Comparing the three graphs an upper and lower bound for the heat recovery exists for the casing angular velocities considered. All three graphs suggest that the heat recovery efficiency has a lower bound (~25%) and the upper bound (~50 %). In addition, ε_R decreases as the casing angular velocity increases, which causes an increase of the mass flow rate through the elevator. For example, for 6 layers of insulation,

increasing the casing angular velocity from 3.4rpm to 7.8rpm decreases the heat recovery from a maximum of 50% to a maximum of 40%, respectively. This behavior is intuitive because as the conveying rate increases less time is available for heat transfer to occur between the auger and the packed bed of sand conveyed up its flights. Furthermore, ε_R, increases slightly as the number

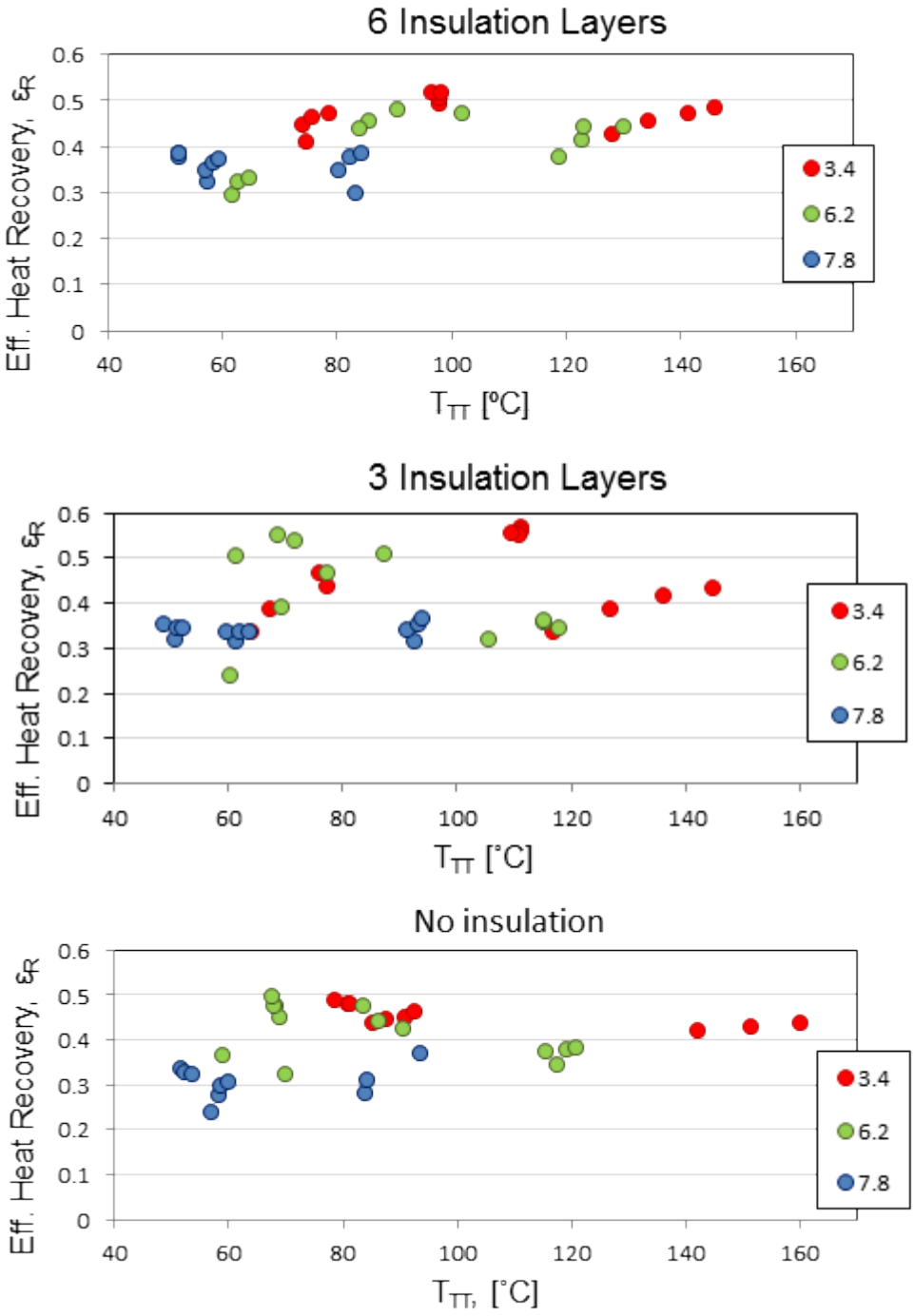

Figure 26. Plots of the effective heat recovery of the PE as a function of the temperature T_{TT}. The three colored markers represent experiments conducted at ω= 3.4rpm, ω= 6.2rpm, and ω= 7.8rpm.

of insulation layers increases. For instance, the experiments conducted at 7.8rpm (blue dots) show ε_R increases from ~30% with 0 layers of insulation to ~37% with 6 layers of insulation. The data for the other casing angular velocities is noisy but an overall increase can be seen as well. Increasing the layers of insulation helps trap heat inside the casing that would otherwise be lost to the environment.

5.3.2. Heat Exchange Power

Figure 27 shows three plots of the heat exchange power, P_{heat}, as a function of T_{TT}. Each plot corresponds to an experiment conducted with a specific number of insulation layers wrapped around the casing. A linear fit was used to compare the behavior of P_{heat} as a function of ω. In all three plots the slope of the linear fit line decreases as ω decreases. This relationship between P_{heat} and ω can be attributed to the direct relationship between the heat exchange power and conveying rate (equation (6)). Additionally, the casing angular velocity affects the temperature range in which P_{heat} reaches its maximum. As ω increases P_{heat} increases much more quickly per change in degree in temperature. The range of heat exchange power values (vertical axis) is fairly constant for all the layers of insulation considered; although a 10W decrease does occur between the 6 layers and no layers of insulation for experiments with ω=3.4rpm. The range of P_{heat} is between ~140W-35W for the casing angular velocities considered. The dependence of the range of P_{heat} on ω signifies that, if a specific P_{heat} value is desired, it can be obtained at a lower temperature by increasing ω.

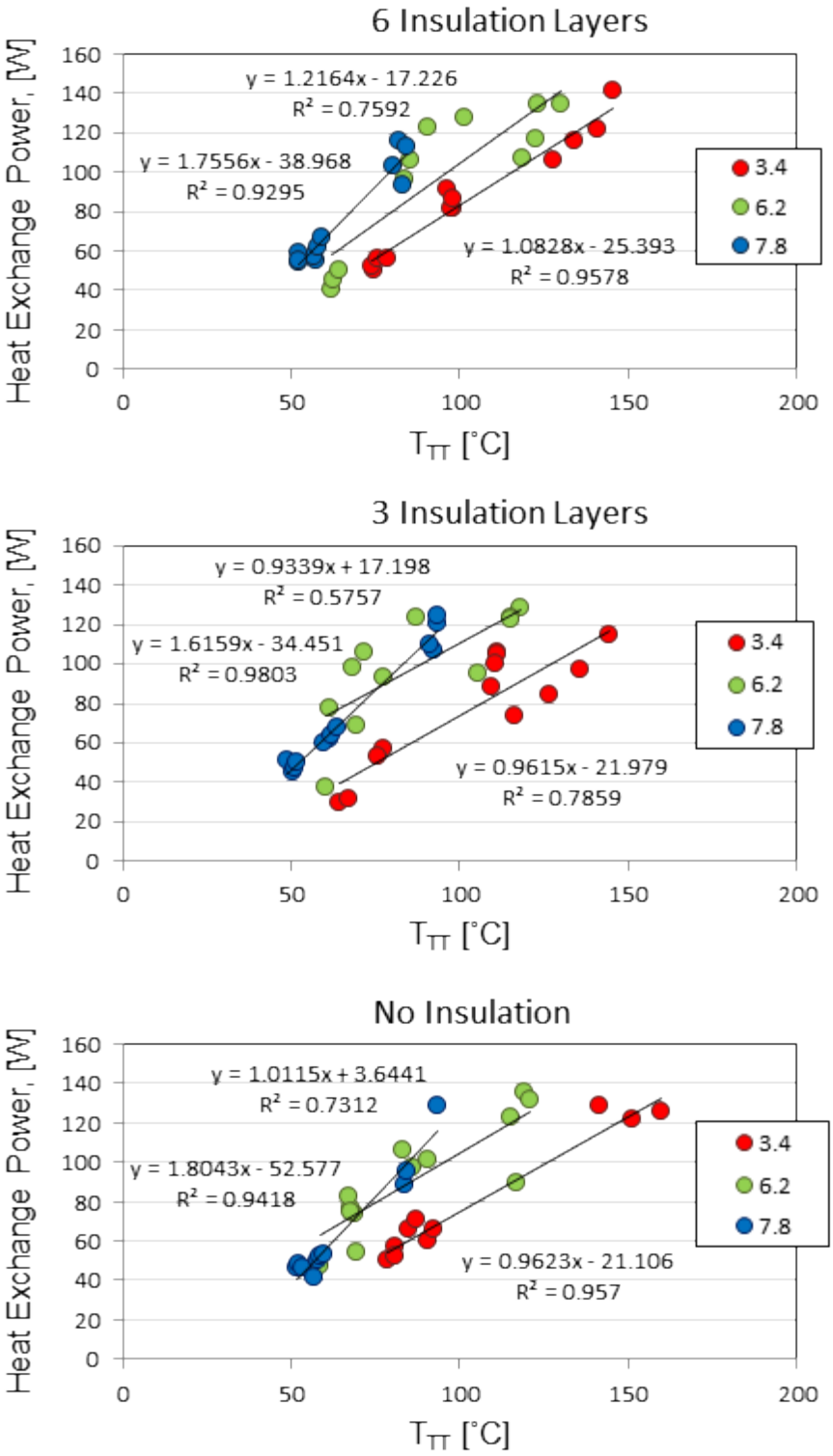

Figure 27. Plots of the heat exchange power as a function of T_{TT}. The colors represent experiments conducted at three different casing angular velocities. For all casing angular velocities considered, as T_{TT} increases heat exchange power increases resulting in more heat being transferred to the cool conveyed sand per unit time.

5.3.3. Effective Heat Loss

Figure 28 shows three plots of the effective heat loss, ε_L, as a function of T_{TT} for three different layers of insulation wrapped around the casing. Each data point color represents experiments conducted at a specific casing angular velocity (given in the legend). In all three plots, the effective heat loss has an upper bound of 50% and a lower bound of 20%. For the slowest casing

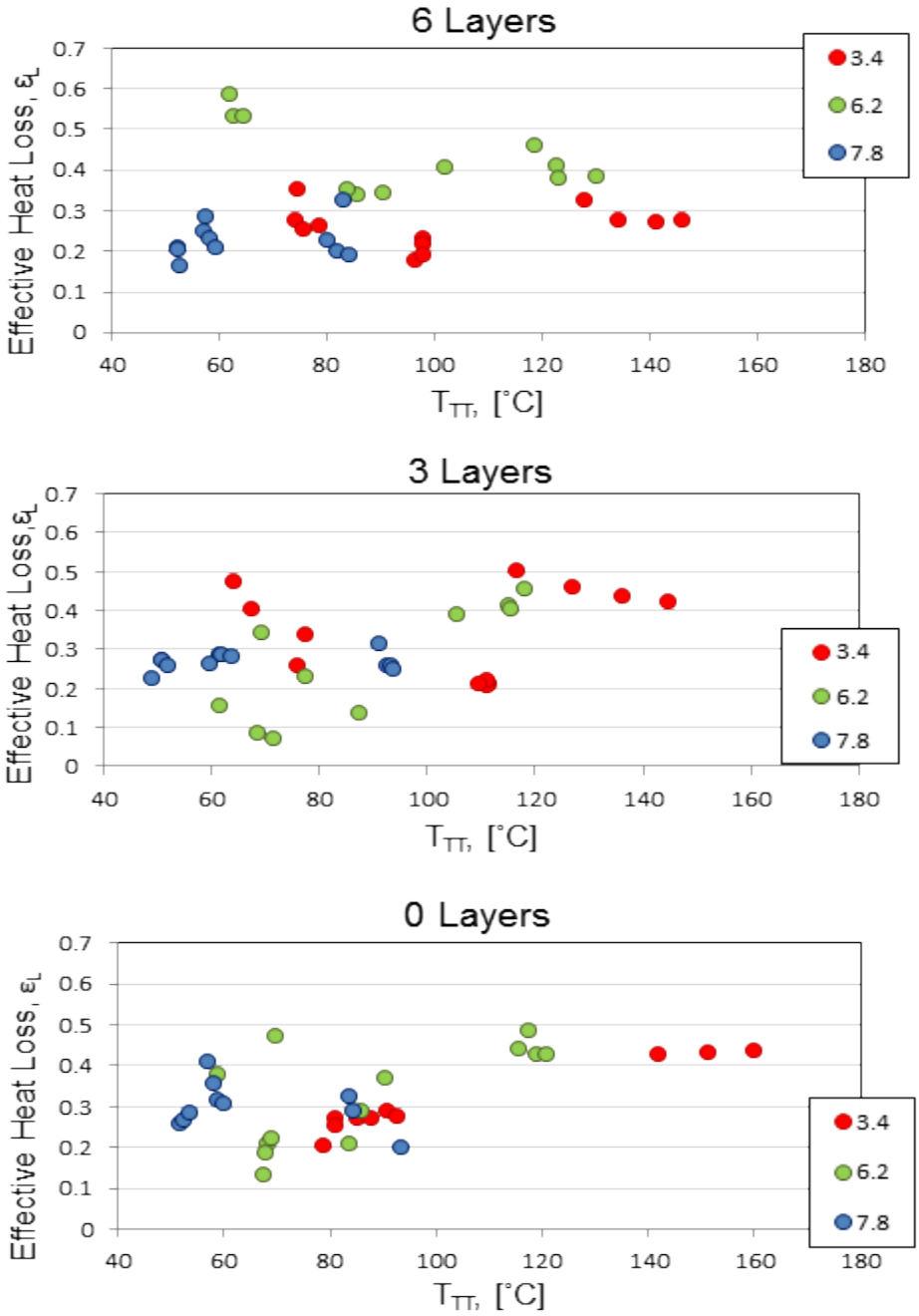

Figure 28. Plots of the effective heat loss as a function of T_{TT}. The three colored markers indicate experiments conducted at three different casing angular velocities: ω= 3.4rpm, ω= 6.2rpm, and ω= 7.8rpm

angular velocities, ε_L decreased as the number of layers increased. For instance, looking at the experiments conducted at a casing angular velocity of 3.4 rpm, ε_L decreased from 40% when using 0 layers to 30 % when using 6 layers of insulation. This behavior is not consistent for all angular velocities. At 7.8 rpm, the average value of ε_L is relatively constant for all three layers of insulation (~25-30%). At greater casing angular velocities, there is less time for heat transfer to occur between particle flows reducing the amount of heat released to the environment. This result implies that the outer layer of sand behaves like a blanket of insulation for higher casing angular velocities.

Considering the relatively high levels of heat loss, it seems likely that heat recovery effectiveness in excess of 75% is feasible in a similar device, with better heat loss control.

6. CONCLUSIONS

In this report, we have presented the evaluation of a viable solid-solid heat recovery particle elevator that uses the Olds Elevator concept, the *compact compound recirculator/recuperator* (C2R2). Four main technical elements were investigated

- An auger design with minimal heat transfer lengths, which nonetheless is capable of efficient particle conveying;
- Particle conveying using a zero-profile cutter compatible with the concentric nesting of multiple elements into a compact device;
- Design solutions for nesting multiple elevators, such that they can work simultaneously and efficiently;
- Heat transfer over distances longer than those indicated by the limitations of static beds.

To design a particle elevator with the above characteristics, each element was evaluated in a series of experimental stages. First, the conveying rate of four multi-flight auger prototypes designed with different number of flights and single flight pitch were measured. The measured conveying rate was used to calculate and compare the augers' conveying efficiencies. Augers with more than 3 flights increased counter torque on the driving motor and casing rotation was not achieved. Due to the increase in counter torque, the A_6 auger (6 flights) did not convey sand for all casing angular velocities. Similarly, the A_4 auger conveyed sand for only one bed depth (3.2 cm). Comparing the results for the A_2, A_3, and A_4 augers suggests that adding flights to the auger increases its ability to exchange heat but has an adverse effect on the conveying rate. Overall the A_2 auger produced the greatest conveying rate between all multi-flight augers considered; however, the difference in conveying rate between the A_2 and A_3 augers decreased as the sand depth increased. The A_2 auger conveyed a minimum 6% greater than the A_3 auger at a bed depth of 15.9cm.

Second, the conveying effectiveness of a zero-profile cutter (ZPC) was evaluated. The ZPC incorporates an innovative cutter design that consists of tapered edges with a thin profile in place of protruding cutters typical of conventional cutters (CNC). The design of the ZPC provides the rigidity needed to reduce fractures that may result from structural weak points such as the cutter/casing joint in the CNC. Additionally, the ZPC is compatible with a tightly nested auger elevator which is needed for the scalability of the particle elevator. The ZPC was successful in conveying sand but was found to produce a much lower conveying rate per unit time than the CNC. The CNC conveyed between 300% - 140% more sand than the ZPC for bed depths between 3 and 16 cm. However, the conveying efficiency of the ZPC was found to be highly effected by the auger design and reached a maximum of ~40% when using the A_2 auger. This result signifies that a maximum conveying efficiency probably exists by choosing an auger with the proper geometry.

Third, the feasibility of a functional nested auger system was demonstrated. The conveying rate for the nested auger system was found to be directly proportional to the casing angular velocity exhibiting the same behavior as a single auger system. A drawback of the design presented is that the concentrically nested augers had to be displaced vertically to preserve the counter-current flow pattern of the single auger elevator. Thus, designing a system with an arbitrary

number of nested augers would be challenging in that several vertical displacements would have to be made. Even with this setback the nested auger elevator was found to be fully functional and conveyed 100% more sand at half the casing angular velocity than the most efficient single auger elevator evaluated in this report.

Finally, the heat recovery between particle flows was evaluated. The maximum heat recovery of ~50% occurred for slower casing angular velocities (~3.4rpm) and the minimum of 25% occurred for faster casing angular velocities (~7.8rpm) signifying that increasing the conveying rate decreases the heat recovery. Overall, the results of the experiment met and surpassed the goals set forth for this project which was to demonstrate that heat recovery >20% was possible. In light of the high heat losses and modest range of evaluated auger geometries, a heat recovery effectiveness of 80% seems feasible in a well-insulated device and with further auger geometry optimizations.

The work presented demonstrates that a mechanically simple solid-solid heat exchanger can be made to achieve high heat recovery between counter-current flows of packed particle beds overcoming the limitations imposed by the low thermal conductivity of the working fluid, particulate matter. In addition, the practicality of the device was demonstrated by showing that it was scalable while preserving the overall flow pattern which makes the device effective in recovering heat. This work is widely applicable to technologies in need of high heat recovery between beds of packed particles such as solar thermochemical fuel production and solar thermochemical energy storage where high heat recovery of concentrated solar energy is essential in producing fuels at competitive costs.

7. REFERENCES

[1] Diver, R. B., Miller, J. E., Allendorf, M. D., Siegel, N. P., and Hogan, R. E., 2008, "Solar Thermochemical Water-Splitting Ferrite-Cycle Heat Engines", Journal of Solar Energy Engineering, 130(4), 041001-1 -041001-8.

2] Ermanoski, I., Siegel, N. P., and Stechel, E. B., 2013, "A New Reactor Concept for Efficient Solar-Thermochemical Fuel Production", Journal of Solar Energy Engineering, 135(3), 031002-1 - 10.

[3] Shapiro, M., Dudko, V., Royzen, V., Krichevets, Y., Lekhtmakher, S., Grozubinsky, V., Shapira, M., and Brill, M., 2004, "Characterisation of powder beds by thermal conductivity: Effect of gas pressure on the thermal resistance of particle contact points", Particle & Particle Systems Characterization, 21(4), 268-275.

[4] GodBee, H. W., and Ziegler, W. T., 1966, "Thermal Conductivities of MgO, Al_2O_3, and ZrO_2 Powder to 850 ° C. I. Experimental", Journal of Applied Physics, 37(1), 40-55.

[5] Golob, M. C., 2011, "Convective Heat Transfer Performance of Sand for Thermal Energy Storage", M.S. Thesis, Georgia Institute of Technology, Atlanta, Georgia.

[6] Murashov, V. V., White, M. A., 2000, "Thermal Conductivity of Cystalline Particulate Materials", Journal of Materials Science, 35(3), 649-653.

[7] McBride, W., Djukic, M., “Experimental Evaluation of the OLDS Elevator Concept”.

DISTRIBUTION

1	MS0899	Technical Library	9536 (electronic copy)
1	MS0359	D. Chavez, LDRD Office	1911


Sandia National Laboratories